OPTIMAL AEROASSISTED INTERCEPT TRAJECTORIES AT HYPERBOLIC SPEEDS

Elmer G. Gilbert*, Robert M. Howe* *, Ping Lu†, Nguyen X. Vinh*
The University of Michigan
Ann Arbor, MI 48109-2140

Abstract

The paper considers the optimization of earth-based multi-stage rocket interceptors with very short flight times and long ranges. The objective is the minimization of the launch mass as a function of interceptor design variables such as: stage size, engine burn times and the angle-of-attack program. Because of the demanding target conditions the payload reaches hyperbolic speeds and the centrifugal force greatly exceeds the gravity force. The minimization of launch mass shows that the needed down-force on the payload is best provided by negative aerodynamic lift. The description and numerical computation of such aeroassisted optimal trajectories is the principal goal of the paper. Topics treated include: a model for the multistage interceptor, the formulation of the optimization problem, the derivation of a *universal curve* which is an accurate model for midcourse segments of the optimal trajectories, effective schemes for parameterizing the angle-of-attack program and procedures for efficient numerical optimization. Results of solution studies are reported. For flight times of six minutes and a range of about 3000 miles, a five-stage interceptor requires a mass ratio of several thousand. The dependence of the mass ratio on key design and target parameters is described.

Nomenclature

A	dimensionless thrust in g's = $T/(m_o g_o)$
C_D, C_L	lift and drag coefficients
D	dimensionless drag force = $\frac{1}{2}\rho v^2 S C_D/(m_o g_o)$
g_0	gravity acceleration at r_o
h	altitude = $r - r_o$
h_S	scale height of exponential atmosphere = 7.16 km
H	dimensionless altitude = h/r_o
i_{SP}	specific impulse
I_{SP}	dimensionless specific impulse = $i_{SP}/(r_o/g_o)^{1/2}$
L	dimensionless lift force = $\frac{1}{2}\rho v^2 S C_L/(m_o g_o)$
m	vehicle mass
m_o	reference mass
M	dimensionless mass = m/m_o
N	number of stages
r	distance of vehicle from center of earth
r_o	reference distance
R	dimensionless distance = r/r_o
S	cross sectional reference area
t	real time
T	engine thrust
v	vehicle speed
V	dimensionless speed = $v/(g_o r_o)^{1/2}$
x	dimensionless time for universal curve
α	angle of attack
γ	flight path angle with respect to local horizontal
η	dimensionless force coefficient = $\rho_o r_o S/m_o$
θ	polar angle of vehicle trajectory
λ	fineness ratio = stage length/stage base diameter
μ	dimensionless inverse scale height = r_o/h_S
$\rho(r)$	atmospheric density
ρ_o	reference density = $\rho(r_o)$
$P(H)$	dimensionless density = $\rho(r_o H + r_o)/\rho_o$
σ_i	mass-ratio parameter for ith stage
τ	dimensionless time = $t/(r_o/g_o)^{1/2}$

I. Introduction

The utilization of satellite-based missles for intercepting ICBM's during their ascent constitutes one of the major efforts in the U.S. Strategic Defense Initiative program. Here, an alternative approach is considered: the use of high performance, multi-stage, earth-based interceptors. The very short flight times and long ranges require hyperbolic speeds and a high ratio of take-off mass to payload mass. A natural objective is the minimization of the mass ratio with respect to interceptor design variables such as: stage size, engine burn times, coasting times between stages and the angle-of-attack program. Since the hyperbolic speeds produce centrifugal forces far in excess of the gravity forces, a net down force on the interceptor is required during its mid-course trajectory. Appreciable reductions in the mass ratio can be acheived if the down-force is generated by negative aerodynamic lift. The optimization and description of such aeroassisted trajectories is the principal goal of this paper. We now summarize the main topics and results.

The paper begins with the details of the model for the multistage interceptor. A number of assumptions are made to keep the complexity of the model within reasonable bounds. After formulating the minimum launch-mass problem, three examples of optimal trajectories are given. They correspond to different assumptions on the trajectory of the final payload: extra-atmospheric flight, atmospheric flight with zero aerodynamic lift, aeroassisted flight. With respect to launch mass aeroassisted flight offers a clear advantage. Optimal aeroassisted trajectories share a common feature. The initial portion of the payload trajectory follows closely a special speed-altitude relationship which is called the *universal curve*. Formulas are derived for the motion along the universal curve. They are useful in understanding the details of the mid-course aeroassisted trajectory and in the numerical solution of the minimum launch-mass problem.

Numerical solution of the optimization problem requires a finite-dimensional parameterization of the angle-of-attack program. To avoid poor conditioning of the resulting finite-dimensional optimization problem, it is essential to do the parameterization indirectly through a direct parameterization of the flight path angle. Various aspects of this procedure are discussed. Finally, some details of the numerical optimization procedure are given.

Many optimal trajectories have been computed. Some of the results are summarized in Section VII. They show the effect on launch mass of such parameters as the time of flight, the intercept altitude, the number of stages and the specific

*Professor of Aerospace Engineering

**Professor of Aerospace Engineering
Associate Fellow, AIAA

†Assistant Research Scientist

impulse of the engines. For 5 and 6 stage interceptors mass ratios on the order of several thousand are necessary. Short flight times and low intercept altitudes increase appreciably the launch mass.

II. Model for the Multistage Interceptor

To obtain the equations of motion it is assumed that all stages of the interceptor are modelled as a point mass moving in a plane which contains the center of a spherical, non-rotating earth with an inverse-square gravitational field. Choosing state variables r, θ, v, γ and m and writing the resulting equations[1] in dimensionless form then gives:

$$\frac{dR}{d\tau} = V \sin\gamma \ , \quad \frac{d\theta}{d\tau} = \frac{V\cos\gamma}{R} \ ,$$

$$\frac{d\gamma}{d\tau} = \frac{1}{V}\left[\frac{A\sin\alpha + L}{M} + \left(\frac{V^2}{R} - \frac{1}{R^2}\right)\cos\gamma\right] \ ,$$

$$\frac{dV}{d\tau} = \frac{A\cos\gamma - D}{M} - \frac{\sin\gamma}{R^2} \ , \quad \frac{dM}{d\tau} = \frac{-A}{I_{SP}} \ . \tag{1}$$

These equations are well scaled when $r_0 \cong$ earth radius and $m_0 \cong$ nominal mass of vehicle. Note $V = 1$ corresponds to the circular orbital speed at r_0 and $\tau = 2\pi$ corresponds to the period of a circular orbit at r_0.

The dimensionless lift and drag forces are given in terms of H and V by

$$L = \frac{1}{2}\,\eta\, P(H)\, V^2\, C_L \ , \quad D = \frac{1}{2}\,\eta\, P(H)\, V^2\, C_D \ . \tag{2}$$

For the results reported later in this paper an exponential variation of density with altitude has been used. This approximation simplifies the computations and produces almost the same optimal trajectories as more complex atmospheric models. For the exponential variation,

$$P(H) = e^{-\mu H} \ . \tag{3}$$

Lift and drag coefficients are modelled by the formulas[2]:

$$C_L = C_N\cos\alpha - C_A\sin\alpha \ ,$$

$$C_D = C_N\sin\alpha + C_A\cos\alpha \ ,$$

$$C_A = 0.13,$$

$$C_L = \sin 2\alpha\cos\tfrac{1}{2}\alpha + 5\,(\pi)^{-1}\,\lambda\sin\alpha\,|\sin\alpha| . \tag{4}$$

In addition to choosing an angle-of-attack program, $\alpha(\tau)$, in (1), it is necessary to specify the thrust program and describe parametrically the physical characteristics of the stages. Our model of the thrust program is simple, and is consistent with the requirements of solid-fuel engines. For the i th stage it consists of an initial coasting period, τ_i^C, where $A = 0$, and a single thrusting period, τ_i^B, where $A =$ constant > 0. The first stage has no coasting period ($\tau_1^C = 0$) and there are N powered stages. The final payload stage is unpowered but may generate a controlled aerodynamic lift. Its coasting time from burnout of the Nth stage to target interception is denoted by τ_{N+1}^C.

The stage masses are modelled as follows. For the i th stage, let M_i^P, M_i^F and M_i^S denote, respectively, the masses of the payload, fuel and structure (together with the engine and other jettisoned components). Then

$$M_i^P = M_{i+1}^P + M_{i+1}^F + M_{i+1}^S, \ i = 0, \ldots, N\text{-}1,$$

M_0^P = launch mass of entire vehicle,

M_N^P = mass of final payload. (5)

Let

$$\sigma_{i+1}\, M_i^P = M_{i+1}^P \ , \ i = 0, \ldots, N\text{-}1. \tag{6}$$

Here, $0 < \sigma_i < 1$, is a stage mass-ratio parameter. Once $\sigma_1, \ldots, \sigma_N$ and M_N^P are specified, the individual stage-payload masses $M_0^P, \ldots, M_{N-1}^P$ are known. To avoid the need for additional stage-size parameters, a final simplifying assumption is made:

$$M_i^S = 0.1\, M_i^F \quad , \quad i = 1, \ldots, N. \tag{7}$$

Then from (4) it follows that

$$M_i^F = (1.1)^{-1}\,(M_{i-1}^P - M_i^P), \quad i = 1, \ldots, N. \tag{8}$$

While (7) neglects many details of the structural design, it is representative of attainable structural efficiencies. Once the fuel masses are determined, the thrust levels A_i can be computed. They are proportional to M_i^F/τ_i^B.

The masses of the stages also affect, through their reference areas, the aerodynamic forces. Let S_i, d_i and λ_i be, respectively, the base area, base diameter and fineness ratio of the i th stage including its payload. Assume that the mass density of each stage prior to the ignition of stage burning is the same. Then, $m_{i-1}^P = (\text{const.})d_i^3\,\lambda_i$. Since S_i is proportional to d_i^2 this gives

$$S_i = C_S\,(m_{i-1}^P\,\lambda_i^{-1})^{2/3},$$

$$= C_S\, m_0^{2/3}\,(M_{i-1}^P\,\lambda_i^{-1})^{2/3}, \ i = 1, \ldots, N+1. \tag{9}$$

We have chosen C_S to make (9) conform closely with the corresponding relation for the Minuteman I vehicle. In our computations $\lambda_i = 10$ for $i = 1, \ldots, N$. Since the final payload is subject to aerodynamic forces during its coast to the target, its reference area, S_{N+1}, and fineness ratio, λ_{N+1}, are needed. This explains $i = N+1$ in (9). In our computations we have chosen $\lambda_{N+1} = 5$.

III. The Optimization Problem

In this section we outline the general features of the optimal interception problem and show by some examples the character of the optimal trajectories. The specified interception data are: the flight time of the interceptor = t_f, the target range angle = θ_f, the target altitude = h_f and the payload mass = m_N^P. The optimization objective is to minimize the total launch mass m_0^P. The free variables are: the angle-of-attack program, the coasting and thrusting periods t_i^C and t_i^B, and the mass-ratio parameters σ_i.

Once the free variables are given it is clear how the corresponding multistage trajectory is generated. Let r_0 = earth's radius. Then the multistage nondimensional equations of motion can be written. For the first stage: $R(0) = 1$, $\theta(0) = 0$, $\gamma(0) = 90°$, $V(0) = 0$, $M(0) = M_0^P$. Since the free variables determine $A(\tau) = A_1$ (through M_1^F and τ_1^B) and M_0^P, the equations of motion can be integrated for $0 \le \tau \le \tau_1^B$. At $\tau = \tau_1^B$ staging occurs and the equations of motion use data appropriate to the second stage. Specifically, (1) is integrated for $\tau_1^B \le \tau \le \tau_1^B + \tau_2^C + \tau_2^B$ with R, θ, γ and V continuous across staging and with $A(\tau)$ determined by A_2, τ_2^C and τ_2^B in the obvious way. The initial mass of the second stage is $M(\tau_1^B) = M_1^P$. The remaining stages are handled in the same way until $\tau = \tau_f = \tau_1^B + \tau_2^C + \tau_2^B + \ldots + \tau_N^B + \tau_{N+1}^C$. Actually, this equation is used to determine τ_{N+1}^C.

Of course, there are constraints on the free parameters:

$$0 < \sigma_i < 1,\ 0 < \bar{\tau}_i^B \le \tau_i^B,\ 0 \le \tau_i^C,\ i = 1, \ldots, N. \qquad (10)$$

The lower bounds, $\bar{\tau}_i^B$, provide a means for limiting the maximum thrust or acceleration of each stage; they may, for instance, depend on other parameters such as M_i^F. In addition to these direct parameter constraints, there are the implicit constraints corresponding to target interception: $\theta(\tau_f) = \theta_f$, $r(\tau_f) = r_f$. In Section VI we indicate how the constraints are implemented in the process of numerically minimizing M_0^P with respect to the free variables.

Another concern in the computations is the representation of the angle-of-attack program. Since $\alpha(\tau)$, $0 \le \tau \le \tau_f$, belongs to an infinite dimensional space, it must be given a finite-dimensional parametric approximation. The details of the parameterization are important and are discussed in Section V.

Operational considerations and the desire to simplify computations may add further constraints to the interception problem. We have, for example, considered three distinct optimization problems. They differ only in the assumptions placed on the motion of the unpowered final stage; the models for the powered ascent stages remain the same. In the first problem, the final payload is constrained to move essentially outside the atmosphere. Thus, the trajectory for the payload is computed easily as a Keplerian transfer from the burnout of stage N to target interception. The constraint is imposed by requiring the minimum altitude of the Keplerian trajectory to exceed a specified altitude. In the second problem, the payload is allowed to move through the atmosphere, but it generates no aerodynamic lift: $\alpha(\tau) = 0$, $\tau_f - \tau_N^C \le \tau \le \tau_f$. This avoids any increase in drag and heating which may result from lift. In the third problem there is no constraint on the payload so that an aeroassisted coasting trajectory is possible.

Figure 1 and Table 1 show typical results for the three problems. The intercept conditions are: $t_f = 360$ sec., $\theta_f = 45°$ (approximately 3100 mi.), $h_f = 400$ km. (approximately 250 mi.), payload mass = $m_N^P = 10$ kg., $i_{SP} = 300$ sec. and N = 5. In general, the optimal coasting periods for the powered stages turn out to be zero. The only exception is the fifth stage of the Keplerian case.

The launch mass is least for the aeroassisted case. There is a simple physical explanation. The short flight time demands hyperbolic speed ($V > \sqrt{2}$) while simultaneously the trajectory must be kept close to the earth in order to intercept the target. To resolve these conflicting demands, a net down force on the vehicle is needed. This force is supplied, without expensive engine thrusting, by negative aerodynamic lift as the payload begins its coast toward the target.

For the zero-lift, atmospheric case negative aerodynamic lift is also exploited, but because of the no-lift constraint on the payload it occurs together with engine thrust in the fifth stage. This accounts for the long burn-time of this stage; it allows more time for the negative aerodynamic lift to act.

In the Keplerian case, the altitude of the payload is constrainted to exceed 100 km. This leads to a very large

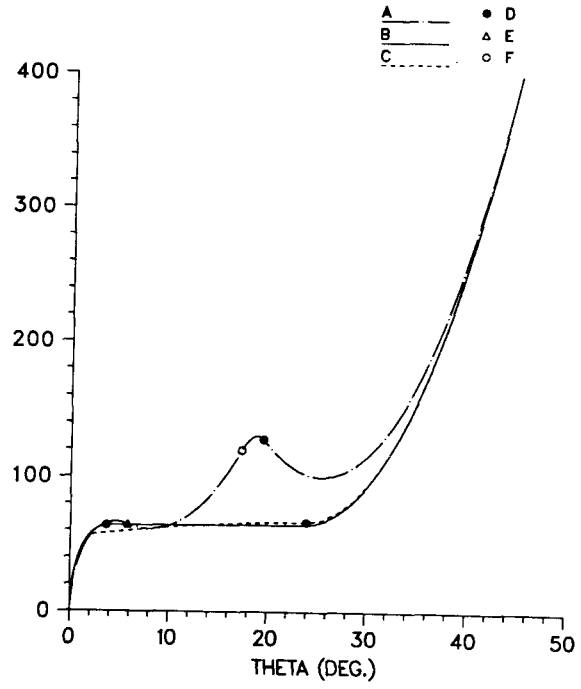

Figure 1 Optimal trajectories for minimum launch mass: A-Keplerian, B-aeroassisted, C-zero-lift atmospheric, D-burnout of fifth stage, E-burnout of fourth stage, F-end of coast for fifth stage. Payload = 10kg.; range angle = 45°; target altitude = 400 km.; flight time = 360 sec..

launch mass because it essentially eliminates effective utilization of negative aerodynamic lift. The Keplerian solution does have a potential operational advantage. Since the trajectory is essentially outside the atmosphere, communication with the payload is not blocked by atmospheric ionization.

IV. The Mid-course Universal Curve

The aeroassisted trajectory in Figure 1 has an obvious mid-course segment on which the final payload coasts for an extended period of time until it begins its rise to the target. On the segment there is a negative aerodynamic lift and the path is nearly horizontal. Such segments have been observed on all optimal aeroassisted trajectories where performance requirements are high, i.e., t_f is small, θ_f is large and h_f is small. Moreover, they can be modelled accurately by a single *universal curve* which relates altitude and speed. This unique relationship is obtained by balancing the difference between centrifugal and gravity forces with negative aerodynamic lift and minimizing the drag losses by choosing the angle of attack

Table 1 Numerical data for optimal trajectories in Figure 1.

			Burnout conditions of 5th stage					Burnout conditions of 4th stage				
Type of Solution	Launch Mass (kg.)	Coasting h (km.)	V	θ (deg.)	γ (deg.)	t (sec.)	Coasting time (sec.)	h (km.)	V	θ (deg.)	γ (deg.)	t (sec.)
Aeroassisted	18,990	63.7	2.11	3.7	0	52.6	0	58.3	1.68	2.2	3.2	40.6
Zero-Lift Atmospheric	23,070	66.5	1.96	24.0	0.005	201.9	0	57.0	1.89	2.5	3.5	42.5
Keplerian	50,720	127.8	2.10	19.5	-4.7	182.0	90.6	64.6	1.82	5.8	-1.6	75.2

which maximizes the lift-to-drag ratio. As will be seen, the time-dependent motion of the payload on the universal curve also has a universal character.

Our development begins with some notation and simplifying parametric assumptions. Let $-C_L^*$ and C_D^* be the lift and drag coefficients which maximize $-C_L/C_D$. They are obtained from (4) and depend only on the fineness ratio, $\lambda = \lambda_{N+1}$, of the payload. Recall that the reference area of the payload, S_{N+1}, is given by (9) and is therefore determined by λ_{N+1} and the mass of the payload, m_N^P. A dimensionless coefficient $C_L^*\eta/2$ plays an important role in the equations which we will consider. It is given by

$$\frac{1}{2}C_L^*\,\eta = \frac{1}{2}C_L^*\,(m_o)^{-1}\,\rho(r_o)\,r_o\,S_{N+1} \tag{11}$$

Since C_L^* and S_{N+1} are fixed by λ_{N+1} and m_N^P, $C_L^*\eta/2$ depends only on m_o and r_o. For the purpose of this section it is convenient to make the following choices for m_o and r_o:

$$m_o = m_N^P, \quad \rho(r_o)\,r_o = \frac{3}{2}m_N^P(C_L^*\,S_{N+1})^{-1}. \tag{12}$$

This gives $M(\tau) \equiv 1$ in (1) and $\frac{1}{2}C_L^*\eta = \frac{3}{4}$.

The required balance of forces on the nearly horizontal trajectory is achieved by setting the normal acceleration, $Vd\gamma/d\tau$, and γ equal to zero in (1) and $C_L = -C_L^*$ in (4). The result is the expression for the universal curve:

$$V = (1+H)^{-1/2}\,[1 - \tfrac{3}{4}(1+H)\,P(H)]^{-1/2}. \tag{13}$$

The reason for choosing r_o by (12) is now clear: (13) contains only one parameter (μ) and at the reference altitude (H=0) the dimensionless speed has a nice nominal value (V=2). Now let P(H) be given by (3). Noting that $\mu \cong 10^3$, it is easy to show that $1.3 \le V \le 4$ implies $|H| \le 0.6 \times 10^{-3}$. Since the expected variation of H is so small, (13) is closely approximated by

$$V = G(H) = (1 - \tfrac{3}{4}e^{-\mu H})^{-1/2}. \tag{14}$$

Even for a non-exponential atmosphere this expression is an excellent representation of (13) because the exponential approximation of P(H) only needs to be accurate for $|\mu H| \le 0.6$, or $|h| \le 0.6\,h_S$. For the payload described in the previous section, r_o corresponds to an altitude of 64.0 km. above the earth's surface.

Along the universal curve there are drag losses and V must decrease. This in turn causes H, θ, γ and α to depend on τ. To obtain these dependencies we begin by substituting (14) into (1) with A = 0:

$$\frac{dV}{d\tau} = G'(H)\frac{dH}{d\tau} = G'(H)\frac{dR}{d\tau} = G'(H)\,G(H)\sin\gamma$$
$$= -D - \frac{\sin\gamma}{R^2} \tag{15}$$

Here, G'(H) is the derivative of G(H) so

$$G'(H) = -\frac{3}{8}\mu\,e^{-\mu H}\,[G(H)]^3. \tag{16}$$

From this expression it is not difficult to verify that $V = G(H) \ge 1.3$ implies $G'(H)\,G(H) > 0.58\,\mu$. Since $\mu \cong 10^3$, $R \cong 1$ and γ is small, the identity on the right side of (15) is closely approximated by

$$D = -G'(H)\,G(H)\sin\gamma. \tag{17}$$

This is the drag required for motion along the universal curve.

By (2) and (4), D defines α and thus C_L. Since the line $C_L = (-C_L^*/C_D^*)C_D$ is the tangent to the lift-drag polar at C_D^*, it is a good approximation for it in the neighborhood of C_D^*. This approximation with D determined by (16) and (17) gives

$$L = -\frac{3}{8}\frac{C_L^*}{C_D^*}\mu\,e^{-\mu H}\,[G(H)]^4\sin\gamma. \tag{18}$$

Substituting (14) and (18) into (1) yields the equations of motion on the universal curve.

To simplify these equations it is assumed with very little error that $\sin\gamma \cong \gamma$, $\cos\gamma \cong 1$ and $R = 1+H \cong 1$. Then

$$\frac{dH}{d\tau} = \gamma\,G(H)\ , \quad \frac{d\theta}{d\tau} = G(H)\ ,$$
$$\frac{d\gamma}{d\tau} = -\frac{3}{8}\frac{C_L^*}{C_D^*}\mu e^{-\mu H}\,[G(H)]^3\,\gamma + G(H) - [G(H)]^{-1}. \tag{19}$$

Because $M(\tau) = 1$ and $V(\tau) = G(H(\tau))$ the order of the original system of equations, (1), has been reduced from five to three. However, the equations (19) are still complicated because they are coupled and nonlinear. Fortunately, the parameter μ is large and this leads to a singularly perturbed system whose solution can be obtained analytically.

The nature of the singularly perturbed problem is revealed more clearly by introducing the scaled variables:

$$\bar{H} = \mu H\ ,\ \bar{\gamma} = \mu\gamma\ ,\ \bar{G}(\bar{H}) = (1 - \tfrac{3}{4}e^{-\bar{H}})^{-1/2}. \tag{20}$$

Then (19) becomes

$$\frac{d\bar{H}}{d\tau} = \bar{\gamma}\bar{G}(\bar{H})\ , \quad \frac{d\theta}{d\tau} = \bar{G}(\bar{H})$$
$$\frac{d\bar{\gamma}}{d\tau} = \mu\{-\frac{3}{8}\frac{C_L^*}{C_D^*}e^{-\bar{H}}[\bar{G}(\bar{H})]^3\,\bar{\gamma} + \bar{G}(\bar{H}) - [\bar{G}(\bar{H})]^{-1}\}. \tag{21}$$

Standard singular perturbation theory can be applied to this system[3] and it shows that the term in the brackets goes to zero quickly and that the remaining, asymptotic, solution satisfies

$$\frac{d\bar{H}_a}{d\tau} = \bar{\gamma}_a\bar{G}(\bar{H}_a)\ ,$$
$$\bar{\gamma}_a = \frac{8}{3}\frac{C_D^*}{C_L^*}e^{\bar{H}_a}\{[\bar{G}(\bar{H}_a)]^{-2} - [\bar{G}(\bar{H}_a)]^{-4}\}. \tag{22}$$

This is a first-order system which can be integrated easily when expressed in terms of the variable $y = [\bar{G}(\bar{H}_a)]^{-1}$.

The details of the integration and back substitution to the original problem variables are lengthy and are omitted. They produce the following formulas for the asymptotic motion along the universal curve:

$$H(\tau) = \frac{1}{\mu}\hat{H}(x)\ ,\ \ \theta(\tau) - \theta(\tau_o) = \frac{C_L^*}{2C_D^*}[\hat{\theta}(x) - \hat{\theta}(x_o)]\ ,$$
$$\gamma(\tau) = \frac{2C_D^*}{C_L^*\mu}\hat{\gamma}(x),\ V(\tau) = \hat{V}(x),\ \ x = x_o + \frac{2C_D^*}{C_L^*}(\tau - \tau_o), \tag{23}$$

where

$$\hat{V}(x) = (3e^x - 1)^{-1}(3e^x + 1)\ ,\ \ \hat{\gamma}(x) = [\hat{V}(x)]^{-2}$$

$$\hat{H}(x) = -\ln\tfrac{4}{3}[1-\hat{\gamma}(x)], \quad \theta(x) = -x + 2\ln\tfrac{1}{2}(3e^{x}-1), \qquad (24)$$

and x_o is determined by $\hat{V}(x_o) = V(\tau_o)$ or, equivalently, by

$$x_o = \ln\tfrac{1}{3}[V(\tau_o)-1]^{-1}(V(\tau_o)+1). \qquad (25)$$

It is easy to confirm that the above formulas cause H and V to lie on the universal curve. Also, using (2), (14), (16), (17) and (24) it follows that

$$C_D = D(\tfrac{1}{2}\eta e^{-\mu H} V^2)^{-1}$$
$$\cong -G'(H)\,G(H)\,\gamma(\tfrac{1}{2}\eta e^{-\mu H} V^2)^{-1} = C_D^*. \qquad (26)$$

Thus, within the accuracy of the approximation $\sin\gamma \cong \gamma$, the motion on the universal curve actually does maximize the lift-to-drag ratio.

The functions $\hat{H}$, $\hat{\theta}$, $\hat{\gamma}$ and $\hat{V}$ are plotted in Figure 2. The ranges of variables which are shown are adequate for any reasonable target conditions. For example, with $C_L^*/C_D^* \cong 2.5$, the value corresponding to $\lambda = 5$, a unit change in $\hat{\theta}$ corresponds to a 72° change in θ. For the entire range which is shown $|\hat{\gamma}| \le 0.61$. This implies $|\gamma| \le 0.61\mu^{-1} \cong 6 \times 10^{-4}$ rad. = 0.034°. The departure of γ from zero is indeed small.

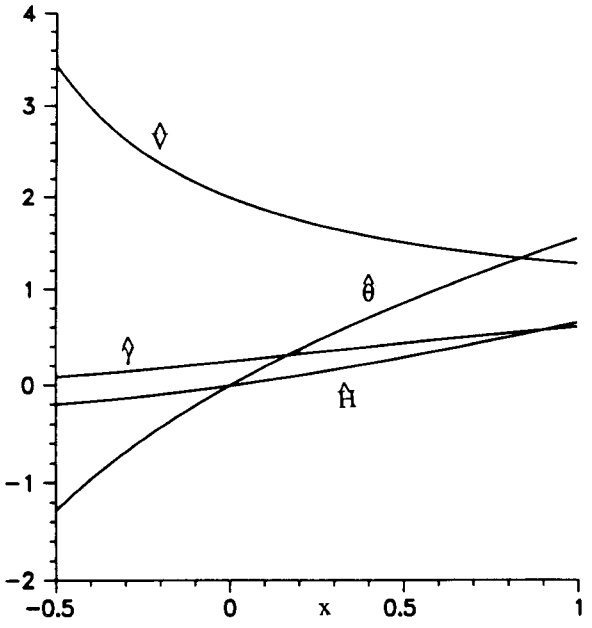

Figure 2 Functions describing motion on the universal curve.

V. The Parameterization of the Angle-of-attack Program

In the formulation of a finite dimensional parametric representation of the angle-of-attack program, several questions arise: the dimensionality of the formulation, its effect on the accuracy of the corresponding approximate optimum solution, its functional form, the incorporation of various constraints, and the conditioning of the resulting numerical optimization problem. These questions are discussed in this section. Our experience shows that relatively low dimensional parameterizations are quite effective, provided they are implemented with care. The dimensionality is important because it has a strong effect on the computational time. Conditioning affects both the speed and reliability of the optimization process. Here, an indirect parameterization of $\alpha(\tau)$ has been crucial to the success of our computations.

A direct parameterization of $\alpha(\tau)$ is the most obvious way to proceed. For example, a continuous piecewise linear function, which is parameterized by its values at its joints (points of slope discontinuity), is simple and has flexibility in that the joints may be place more closely in those intervals where $\alpha(\tau)$ is expected to vary most rapidly. Alternatively, polynomial representations for each of the stages may be used. The fatal shortcoming of such direct parameterizations is poor conditioning of the optimization problem. The terminal constraints are very sensitive with respect to small changes in $\alpha(\tau)$, especially when the changes occur early in the flight. This is not surprising in view of the open-ended integrations which occur in solving the equations of motion.

To circumvent the poor conditioning, it is better to parameterize $\alpha(\tau)$ indirectly through a direct parameterization of $\gamma(\tau)$. In this approach, $d\gamma/d\tau$ is computed from the parameterized $\gamma(\tau)$ and substituted, together with R, γ, V and M, into the third equation of (1). This equation then becomes through $\sin\alpha$ and L an implicit equation in α. The indirect parameterization of α is obtained by solving the implicit equation. Note that this eliminates the need to integrate the differential equation in γ; of course, the remaining differential equations must be integrated as usual. When the indirect parameterization is used, the entire trajectory is under more direct control. Changes in $\gamma(\tau)$ near the beginning of the trajectory have very little effect on the terminal portions of the trajectory. Thus, the sensitivity of the terminal constraints to the parameterization is greatly reduced. Another advantage, perhaps less important, is evident at launch. Here, the differential equation for $d\gamma/d\tau$ has a singularity because V = 0. With the γ parameterization the differential equation is not integrated and the normally troublesome singularity is avoided.

The implicit equation for α presents possible difficulties. An inadmissible $\gamma(\tau)$ may be specified, i. e., one in which the implicit equation has no solution. This corresponds physically to requiring more transverse acceleration than is available. In most of our work inadmissibility has not been a problem, provided the line search in the optimization algorithm has a procedure for reducing step size when it produces an inadmissible $\gamma(\tau)$. Occasionally, when α must be very large, as in the fifth stage of the Keplerian problem of Figure 1, it is better to parameterize $\alpha(\tau)$ directly, keeping the γ parameterization for the other stages. The actual numerical solution of the implicit equation is straightforward. One approach is to use several Newton iterations. Alternatively, L may be approximated by a quadratic function of $\sin\alpha$; then the implicit equation is quadratic in $\sin\alpha$ and it may be solved by formula.

Another issue is the smoothness of $\alpha(\tau)$ and other problem variables. If $\gamma(\tau)$ is continuous but has slope discontinuities, as in the case of a piecewise linear parameterization, the differentiation of $\gamma(\tau)$ causes $\alpha(\tau)$ to be discontinuous. Even for smoother parameterizations the problem is not avoided. At the staging times the vehicle mass, thrust and aerodynamic parameters change discontinuously and this causes discontinuities in $\alpha(\tau)$. Continuity of $\alpha(\tau)$ can be imposed by introducing an appropriate jump in $d\gamma/d\tau$ at the staging time. The value of $d\gamma/d\tau$ just after staging, $(d\gamma/d\tau)^+$, is evaluated by using its defining equation, (1), with R, γ, V and α continuous across staging and the changes in M, A and aerodynamic parameters determined by the staging equations of Section II.

It is also possible to introduce other smoothness constraints. For example, consider the pitch angle, $\psi = \alpha + \gamma$. Although ψ does not appear in the point mass equations, it has practical implications because the moment applied to the vehicle is proportional to its second derivative. To avoid an impulsive moment it is necessary to require continuity of $d\psi/d\tau$. This leads to the condition: $(d\alpha/d\tau)^+ - (d\alpha/d\tau)^- =$

$(d\gamma/d\tau)^+ - (d\gamma/d\tau)^-$, where the superscripts give the values immediately before and after staging. In order for the derivatives with respect to α to exist, it is certainly necessary that $\alpha(\tau)$ be continuous. Thus, as in the previous paragraph, both $(d\gamma/d\tau)^+$ and $(d\gamma/d\tau)^-$ are known. The resulting condition on $(d\alpha/d\tau)^+ - (d\alpha/d\tau)^-$ can be obtained by differeniating the $d\gamma/d\tau$ equation once. This in turn defines the value of $(d^2\gamma/d^2\tau)^+$. Thus, conditions on both $(d\gamma/d\tau)^+$ and $(d^2\gamma/d^2\tau)^+$ are obtained.

Based on our numerical experience, a few remarks on the functional form of the γ parameterization are in order. Because of the large changes in γ encountered in the first stage it has been found necessary to use a parameterization with at least three free parameters. Since $\gamma(0) = 90°$, a cubic in τ satisfies this requirement and has been as effective as any other choice. For the remaining stages, one free parameter suffices. When there are no smoothness constraints, a linear function works well. Only one parameter is involved for each stage because $\gamma(\tau)$ must be continuous across staging. When continuity constraints are imposed, a more elaborate, one-parameter representation is needed. For instance, when $d\psi/d\tau$ is continuous, we have found it effective to use $\gamma(\tau) = a + b\tau + ce^{-\sigma\tau} + de^{-\nu\tau}$. The parameters c and d allow the matching of the constraints on $(d\gamma/d\tau)^+$ and $(d^2\gamma/d^2\tau)^+$. The values σ and ν are chosen so that the effect of the continuity conditions does not persist for too long a period of time. For a given functional form, the free parameters may be defined in different ways. It has been found that problem conditioning is usually better if values of γ at specified interpolation points are used. For example, when there is one free parameter for a stage, the value of γ at the termination time is a good choice.

VI. Details of the Numerical Optimization Procedure

In this section the main details of the numerical optimization procedure are reviewed briefly. Our general approach involves the formulation of a finite dimensional optimization problem with equality constraints and the solution of this problem by augmented-Lagrangian, quasi-Newton techniques.

The variables in the finite dimensional optimization problem include the stage mass-ratio parameter, σ_i, the stage burn time, τ_i^B, and the stage coast time, τ_i^C, for i = 1,....,N. The constraints, (10), on these parameters are implemented by means of nonlinear transformations such as

$$\sigma_i = (1 - \varepsilon)(.5 + .5 \sin \phi_i), \tag{27}$$

and

$$\tau_i^B = 0.5(\bar{\tau}_i^B + \tilde{\tau}_i^B) + 0.5(\bar{\tau}_i^B - \tilde{\tau}_i^B) \sin \upsilon_i . \tag{28}$$

In (27), ε is a small positive number which implements the strict inequality on σ_i. The variables ϕ_i and υ_i become unconstrained variables in the finite dimensional optimization problem. The parameter $\tilde{\tau}_i^B$ is a scaling parameter which is an upper estimate for τ_i^B that causes $\bar{\tau}_i^B \le \tau_i^B \le \tilde{\tau}_i^B$ for $-\pi/2 \le \upsilon_i \le \pi/2$. Such scaling techniques improve the numerical conditioning of the optimization problem when problem parameters have widely different ranges of values. The nonlinearities introduced by the transformations do not appear to affect the speed or reliability of the numerical optimization process. The remaining variables in the finite dimensional optimization problem are the parameters needed for the representation of the angle-of-attack program, as described in the previous section. The cost to be minimized is M_0^P, obtained from the σ_i by (6).

The equality constraints in the numerical optimization problem include the target conditions $\theta(\tau_f) = \theta_f$ and $R(\tau_f) = R_f$. Errors in meeting these conditions are evaluated by integrating the differential equations of motion, which are fully defined once the variables of the preceding paragraph are specified. In the case of the zero-lift, atmospheric problem, the trajectory of the final payload is determined by integrating the equations of motion from the time of last-stage burnout, τ_b, to τ_f with $\alpha(\tau) = 0$ and A= 0. Of course, the effects of aerodynamic drag must be taken into account. If coasting of the powered stages is not allowed and the guidelines of the preceding section are followed, there is a total of 3N +2 variables: N each for (27) and (28), 3 for the parameterization of γ in the first stage and 1 for the parameterization of γ in each of the remaining stages.

For the aeroassisted problem the universal curve is used. This eliminates the need to parameterize the angle-of-attack program and integrate the equations of motion during the mid-course coast. At the time of final-stage burnout, $V(\tau_b)$ is known. By setting $\tau_0 = \tau_b$, formulas (23)-(25) define the motion along the universal curve. In general the conditions $V(\tau_b) = G(H(\tau_b))$ and $\gamma(\tau_b) = \gamma_a(\tau_b)$ are not satisfied by the ascent trajectory, so they must be imposed as additional equality constraints. The universal curve is followed until a time $\tau = \tau_d$ is reached. After this time $\alpha(\tau)$ is set to zero. Because there is no aerodynamic lift and V> 1, the trajectory then departs from the universal curve and rises toward the target. By evaluating this departure trajectory at $\tau = \tau_f$, the errors in the target conditions are determined. Since $\gamma_a(\tau_b)$ is extremely small, there is little error if $\gamma(\tau_b) = \gamma_a(\tau_b)$ is replaced by $\gamma(\tau_b) = 0$. This reduces by one the number of variables used in the parameterization of γ for the Nth stage and reduces the total number of equality constraints from four to three. If the assumptions of the preceding paragraph hold, the total number of variables is again 3N + 2. The elimination of one γ parameter is balanced by the addition of the parameter τ_d.

To implement the numerical minimization it is also necessary to evaluate the gradients of the constraint functions and the launch mass. Since the constraint functions are obtained by integrating complex nonlinear differential equations, it is extremely difficult to write equations for their partial derivatives. Thus, we have used first order finite difference formulas. This is numerically expensive because each evaluation of the gradient requires n + 1 integrations of the differential equations, where n is the number of variables. Techniques for speeding the computations have been report by Howe et. al.[4]. Rounding and truncation errors in the computation of the gradients can seriously degrade the performance of the minimization algorithm. In this regard the naturally good scaling of the dimensionless equations (1) is a distinct advantage. Balancing the rounding and truncation errors by a proper choice of the finite difference increment is also important[5].

The minimization program used in our computations is a variant of the BFGS, quasi-Newton implementation due to Shanno and Phua[6]. As mentioned earlier, a precaution has been taken to reduce the likelihood that an inadmissible $\gamma(\tau)$ will be produced by the line search. To eliminate gradient evaluations in the line search, the derivative of the cost function in the search direction is computed directly by a finite difference formula. Also, a procedure has been added which greatly reduces the probability that the descent will terminate prematurely due to accumulation of round-off errors in the quasi-Newton update. The equality constraints are treated by the augmented Lagrangian method. Both the penalty coefficients and the multipliers are updated automatically by a scheme which is described by on page 134 of Fletcher[7].

Generally, the performance of the overall optimization procedure has been very satisfactory. The number of gradient evaluations required to obtain a solution is between 300 and 400. This is not unreasonable for the number of problem variables: 17 for N = 5 and 20 for N = 6. Errors in meeting the specified target conditions are very small: about 1 meter in altitude and about 0.05° in range angle. The computational time for a solution is typically between 60 and 90 minutes on an Apollo DN 4000.

(a)

Angle of attack in degrees

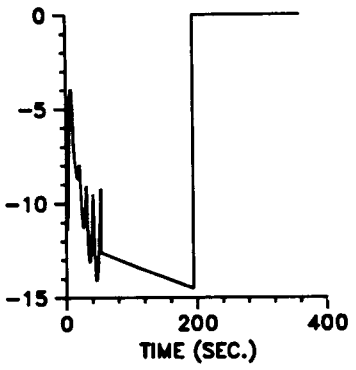

(b)

Speed in units of circular orbital speed at the earth's surface

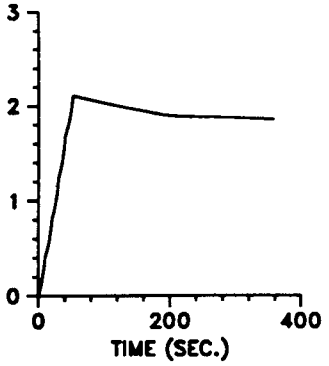

(c)

Logarithm of launch mass in kg.

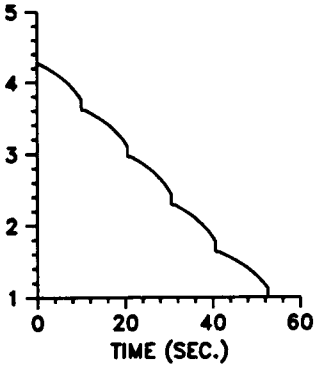

(d)

Acceleration of vehicle in g's

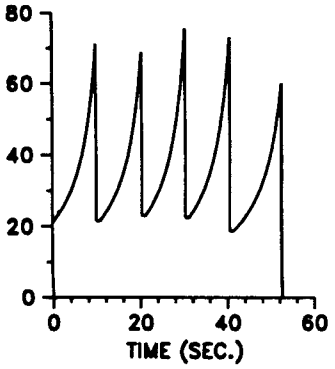

(e)

Flight path angle in degrees

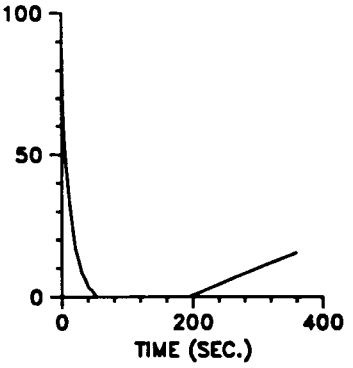

(f)

Flight path angle in degrees

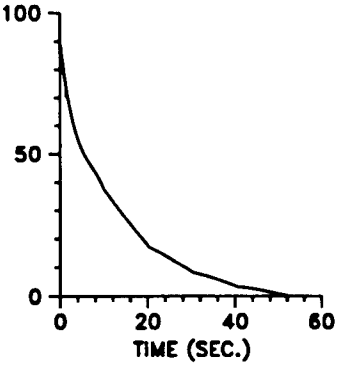

(g)

Angle of attack in degrees

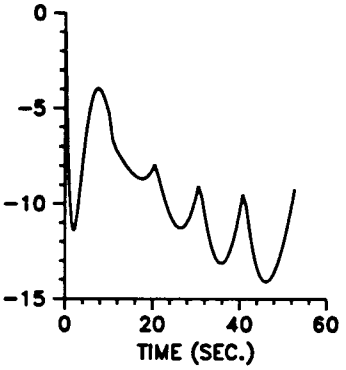

Figure 3 Additional details of the optimal aeroassisted trajectory shown in Figure 1.

VII Some Specific Results

Many optimal intercept problems have been solved using the methods and models of the preceding sections. In this section we summarize some of our results for the aeroassisted problem. The pitch angle is constrained to have a continuous derivative except at the entry and exit points of the universal curve, where $\alpha(\tau)$ is allowed to be discontinuous. A variety of problems have been solved where coasting of the stages is allowed. In these problems the optimal coasting times are either zero or so small that they have little effect on the optimal launch mass. For all the problems considered here the coasting times have been set to zero. The minimum burn time for each stage is 10 seconds and the payload mass is 10 kg. Except for the results in Figure 6, the specific impulse is fixed at 300 seconds.

Additional details of the optimal aeroassisted solution described in Section III are shown in Figure 3. The staging times are apparent. With the exception of the fifth stage, the optimal burn times are at their lower limits of 10 seconds. The resulting vehicle acceleration A/M is quite high, ranging from about 20 to 70 g's. If the minimum burn time is reduced below 10 seconds, even higher accelerations are obtained. The universal curve is followed from about 53 seconds to 194 seconds. The slight drop in V predicted by Figure 2 is evident. There is little loss in speed after the exit from the universal curve. The reason is obvious from Figure 1: the trajectory leaves the atmosphere quickly, so there is little aerodynamic drag. Plots (f) and (g) of Figure 3 show in greater detail the flight path angle and and the angle of attack during ascent. On close inspection the linear-exponential parameterization of $\gamma(\tau)$ is discernable in plot (f). If the smoothness constraint on the pitch angle is removed and $\alpha(\tau)$ is allowed to be discontinuous at the staging points, the overall character of the trajectory is essentially the same and the launch mass is changed by about 0.5 %. Thus, the smoothness of the pitch angle does not seem to be a very stringent constraint.

Figures 4 through 6 illustrate the effect of key parameters

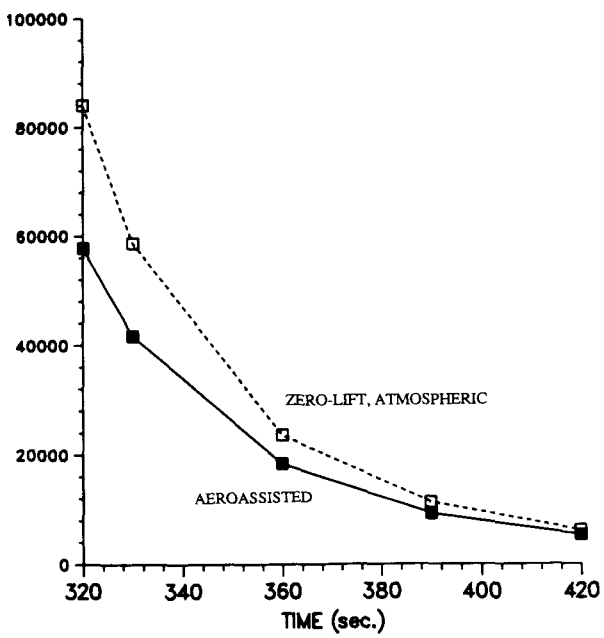

Figure 4 Optimal launch mass in kg. as a function of flight time. Number of stages = 5; payload = 10 kg.; range angle = 45°; target altitude = 200 km.; specific impulse = 300 sec..

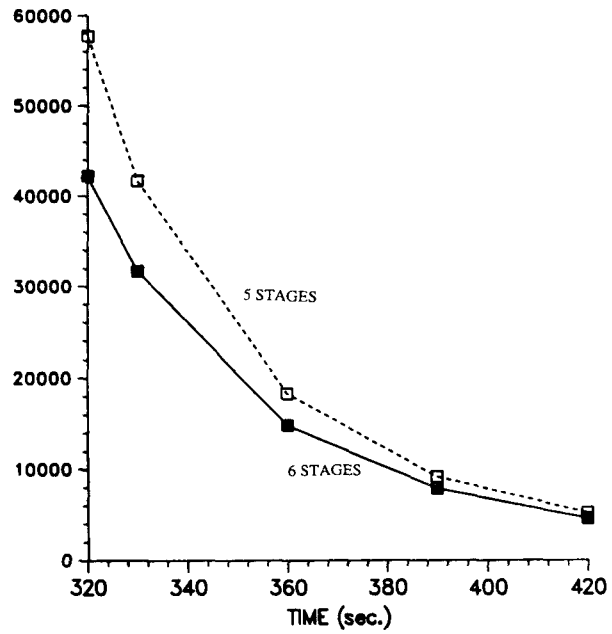

Figure 5 Optimal launch mass in kg. as a function of flight time for aeroassisted trajectory. Payload = 10 kg.; range angle = 45°; target altitude = 200 km.; specific impulse = 300 sec..

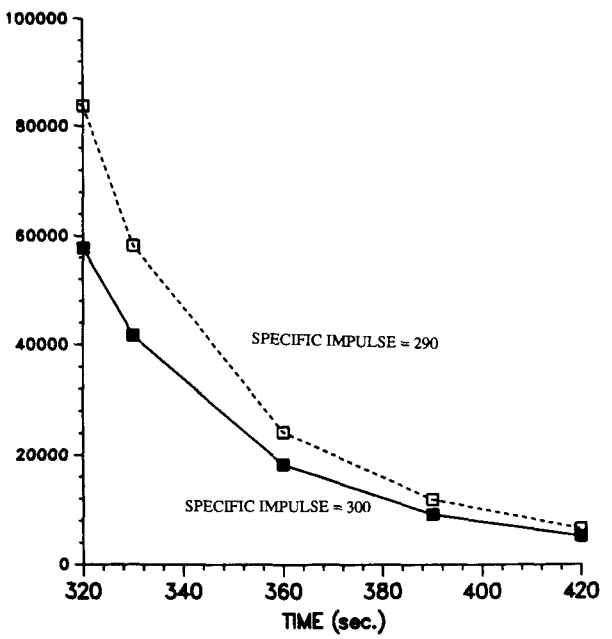

Figure 6 Optimal launch mass in kg. as a function of flight time for aeroassisted trajectory. Number of stages =5; payload = 10 kg.; range angle = 45°; target altitude = 200 km..

on the optimal launch mass. Note that the target altitude is 200 km., a more demanding intercept condition than the 400 km. of the preceding problem. Figure 4 shows the relative performance of optimal aeroassisted trajectories and optimal zero-lift, atmospheric trajectories. The advantage of the aeroassisted trajectories is greater for shorter intercept times. For both types of trajectories the launch mass grows very rapidly as the flight time approaches 320 seconds. Figure 5 shows the difference between 5 and 6 stage aeroassisted interceptors. The 6 stage interceptor has a decided advantage for the shorter flight times. Figure 6 shows the affect of reducing the specific impulse. The 10 second reduction increases the launch mass by over 40 % for the shorter flight times.

Additional solution results for the aeroassisted case suggest other trends. If all other parameters are fixed, the optimal launch mass varies little if the range angle and intercept time vary in direct proportion. Increasing the axial drag coefficient, C_A , by 0.02 increases the launch mass by about 10 %. Increasing the mass density of the stages by 50 % decreases the launch mass by about 6 %.

Acknowledgement

The research reported in this paper has been supported by the U. S. Army Strategic Defense Command under contract number DASG60-88-C-0037. The authors wish to thank David Parag for his helpful contributions.

References

(1) N. X. Vinh, A. Buseman and R. D. Culp, *Hypersonic and Planetary Entry Flight Mechanics*, The University of Michigan Press, Ann Arbor, Michigan, 1980.

(2) L. H. Jorgensen, "Estimation of Aerodynamics for Slender Bodies Alone and with Lifting Surfaces," *AIAA Journal*, Vol. 11, No. 3, 1975, pp. 409-412.

(3) R. E. O'Malley, Jr., "On Nonlinear Singularly Perturbed Initial Value Problems," *SIAM Review*, Vol. 30, No. 2, 1988, pp. 193- 212.

(4) R. M. Howe, E. G. Gilbert, Ping Lu and N. X. Vinh, "Trajectory Optimization of Earth-launched Interceptors at Supercircular Speeds," *Proceedings of the International Society for Optical Engineering*, Vol. 872, 1988, pp. 12-18.

(5) P. E. Gill, W. Murray and M. H. Wright, *Practical Optimization*, Academic Press, New York, 1981.

(6) D. F. Shanno and K.H. Phua, "Minimization of Unconstrained Multivariate Functions," *ACM Transactions on Mathematical Software*, Vol. 6, 1980, pp.618-622.

(7) R. Fletcher, *Practical Methods of Optimization*, Vol. 2, Wiley-Interscience, New York, 1981.